Strong remanent magnetization in pyrrhotite: A structurally controlled example from the Paleoproterozoic Tanami orogenic gold province, northern Australia

Nicholas G. Direen [a,b,*], Kate M. Pfeiffer [a,c], Philip W. Schmidt [d]

[a] *School of Earth & Environmental Sciences, University of Adelaide, Adelaide, SA 5005, Australia*
[b] *School of Earth Science, University of Tasmania, Private Bag 79, Hobart, TAS 7001, Australia*
[c] *Newmont Australia Pty Ltd., Adelaide, SA, Australia*
[d] *CSIRO Exploration & Mining, North Ryde, NSW 1670, Australia*

ARTICLE INFO

ABSTRACT

Rocks associated with an orogenic gold system in the Paleoproterozoic Granites/Tanami Inlier of northern Australia exhibit strong natural remanent magnetism, identifiable in regional aeromagnetic data.

Petrographical analysis indicates the two dominant magnetic minerals in the rocks of this region are multidomain magnetite and monoclinic pyrrhotite. Chemical analysis using an electron microprobe has determined that the magnetite and pyrrhotite are stoichiometrically pure, without significant elemental substitution. Alternating field demagnetization, Curie Temperature, and hysteresis analysis indicates that the remanently magnetized phase is monoclinic pyrrhotite with low magnetic susceptibility. In contrast, multidomain magnetites lack remanence and have high magnetic susceptibilities.

Pyrrhotite is preserved in the rock mass along with other sulfide minerals as millimeter-scale veins parallel to regionally developed, penetrative mylonitic shear bands (c-planes) formed during sulfide remobilization in the waning, cooling stages of hydrothermal Au deposition. In contrast, magnetite grains exhibit porphyroblastic textures, consistent with formation during prograde to peak metamorphism, indicating formation prior to pyrrhotite, earlier in the orogenic cycle. Because of the low Curie Temperature (*ca.* 325 °C) of pyrrhotite, it is therefore likely that remanent magnetization effects observed in aeromagnetic images of the Tanami Inlier, are associated with structures intimately related to the late stages of Au mineralization during retrograde greenschist metamorphism after the peak thermal point of the orogenic cycle.

© 2008 Elsevier B.V. All rights reserved.

1. Introduction

The focus of magnetic studies in mineral exploration is usually the acquisition and processing of data, with less emphasis on the actual mineralogical sources, or paragenetic sequences that combine to produce magnetic anomalies in rocks (Clark, 1997). A common assumption made when interpreting aeromagnetic surveys is that the mineral creating induced magnetic anomalies is magnetite (e.g. Pucher, 1994; Shive et al., 1992). Generally, this assumption holds (e.g. Whiting, 1986), but when there are non-induction dipole, high amplitude anomalies, it is necessary to determine the mineralogical source(s) of the magnetic signature (e.g. Airo, 2002; Alva-Valdivia et al., 2003a,b).

This is because these unusual anomalies can arise from the magnetizations of many different individual magnetic minerals, or combinations thereof (e.g. single domain magnetite, pyrrhotite, titanomagnetite, titanohematite, maghemite: (Clark, 1997)). However, excepting magnetite, the effects of these minerals are reported in relatively few case studies (e.g. Airo, 2002; Airo and Loukola-Ruskeeniemi, 2004; Clark and Tonkin, 1994; Kelso et al., 1993; McEnroe and Brown, 2000; Pucher, 1994).

Monoclinic pyrrhotite is a ferrimagnetic mineral (Clark, 1997) which can hold a strong remanent magnetism (Henkel, 1994), and large concentrations (several wt.%) of ferrimagnetic, monoclinic pyrrhotite in a rock are one possible source of unusual negative anomalies in aeromagnetic datasets (Henkel, 1994; Pucher, 1994; Airo, 2002). Monoclinic pyrrhotite is relatively rarely developed in rock masses, due to the physico-chemical circumstances in which it forms (Clark, 1997; Airo, 2002). In this paper, we present a case study investigating the source of unusual negative magnetic anomalies, and where multidomain magnetite and monoclinic pyrrhotite have formed distributed through a rock mass during different stages of Paleoproterozoic tectonic evolution of the rock system sourcing the magnetic anomalies. This evolution included a period of significant Au mineralization. Hav-

* Corresponding author at: School of Earth Science, University of Tasmania, Private Bag 79, Hobart, TAS 7001, Australia. Fax: +61 2 62834801.
E-mail address: n_direen@utas.edu.au (N.G. Direen).

ing established the source(s) of the non-induction anomalies, we then investigate their relationship to Au-forming events that were penecontemporaneous with different stages of magnetic mineral growth.

2. Geological setting

The Paleoproterozoic Tanami Orogenic gold province is located in The Granites/Tanami Inlier, Northern Territory (Fig. 1). The Granites/Tanami Inlier is situated to the west of the Wiso Basin and to the north of the Arunta Block (Fig. 1), 600 km north-west of Alice Springs.

The stratigraphic succession of The Granites/Tanami Inlier is summarised in Fig. 2. The oldest known rocks in this region are Archean gneisses, dated at 2510 Ma (Wygralak et al., 2001) (Fig. 2). Overlying the Archean basement is the Paleoproterozoic Tanami Group, comprising the basal Dead Bullock Formation and overlying Killi Killi Formation. The Dead Bullock Formation has been further subdivided into the Blake Beds and Davidson Beds, which are conformable (Smith et al., 1998), but differentiated on chemical and sedimentary differences (Voulgaris and Emslie, 2004). The Blake Beds are dominated by carbonaceous, fine-grained pelite with rare chert horizons (Smith et al., 1998), and are host to the major Callie gold deposit. The Orac Formation within the Davidson Beds hosts the Villa, Fumarole and Avon gold deposits (Smith et al., 1998).

The rocks of The Granites/Tanami Inlier underwent complex polyphase deformation in the Tanami Orogeny from 1835 Ma to 1820 Ma, followed by emplacement of granitic intrusions from 1820 Ma to 1790 Ma (Crispe et al., 2002). The latter event also included the emplacement of The Granites Granite, which intruded *ca.*1791 ± 4 Ma (Cross et al., 2005). Following the Tanami Orogeny, the Pargee Sandstone was deposited over the deformed Tanami Group (Nicholson, 1990), with detrital zircons from the latter succession dated at 1768 ± 14 Ma (Cross et al., 2005).

From 1720 Ma to 1670 Ma, gold was deposited by a widespread hydrothermal event (Wygralak et al., 2001). This event was not temporally related to older granitoid magmatism, but was part of a larger scale tectonic event that produced deformation in the North,
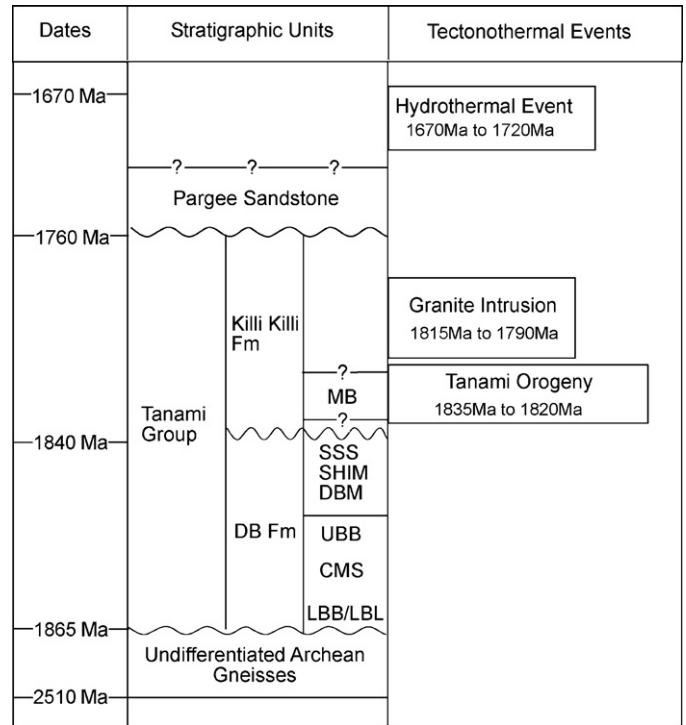

Fig. 2. Geological units and tectonothermal events within the Tanami Orogenic gold province. (MB, Madigan Beds; DB Fm, Dead Bullock Formation; SSS, Seldom Seen Schists; SHIM, Schist Hills Iron Member; DBM, Dead Bullock Member; UBB, Upper Blake Beds; CMS, Callie Mine Stratigraphy; LBB/LBL, Lower Blake Beds/Lower Blake Lode).
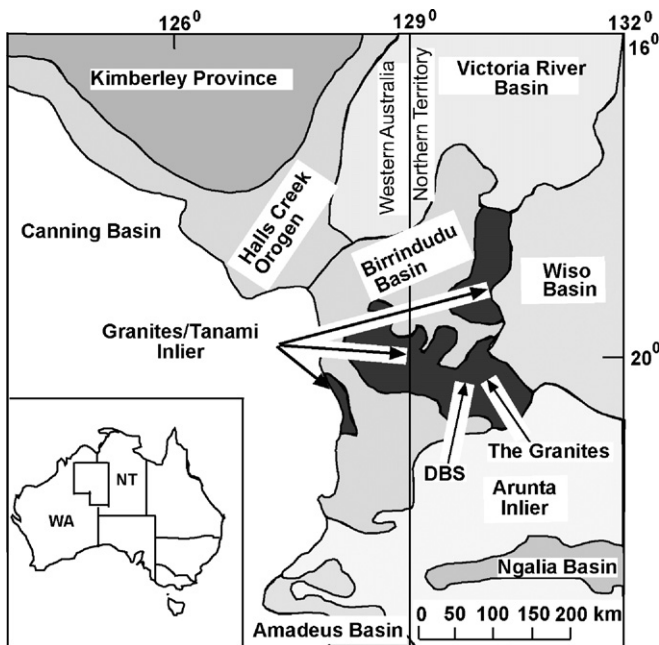
Western and Southern Australian Cratons (Kerim-Sener et al., 2005) (Figs. 2 and 3). Four main gold districts from this event are now preserved within the Inlier. Each displays variations in mineralization styles, depth of emplacement and metamorphic grade. A summary of the deposit styles in the study area is shown in Fig. 3.

Structurally, the evolution of The Granites/Tanami Inlier area has recently been summarised by Crispe et al. (2007). They showed that the large-scale regional architecture around The Granites–Dead Bullock Soak area is dominated by steeply plunging, approximately E- to SE-trending isoclinal folds formed during the Tanami Orogeny. These produce quite steeply dipping (up to 80°) bedding and cleavage planes through the region. These folds are overprinted in localised areas by three further phases of folding of various styles, producing localised folds with crenulation of earlier cleavages in the hinge zones (Crispe et al., 2007). A subsequent regional left-lateral transpressional event then overprinted the system in association with the gold hydrothermal event; this produced N- to NW striking shear zones across the region, associated with penetrative ductile fabric development. Late brittle faulting from subsequent Mesoproterozoic and Palaeozoic tectonism is also observed locally in some areas.

In general, the complex ductile refolding and shearing of the original stratigraphy and the overprinting gold mineralization, means that the original architecture of particular horizons is virtually impossible to restore in detail. This is especially so in the sulfide-rich horizons associated with Au ores, which are particularly incompetent compared to the wall rocks (e.g. Adams, 1997), and thus prone to being "smeared out" to form composite S0/x foliations in localised, centimeter to millimeter-scale shear-zone fabrics. The difficulty of determining the relationship of given stratigraphic, structural or mineralogical horizons to magnetic anomaly maps is compounded by the relative sparseness of drill holes regionally.
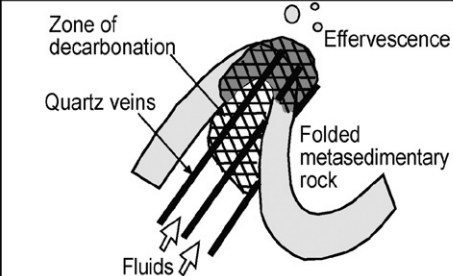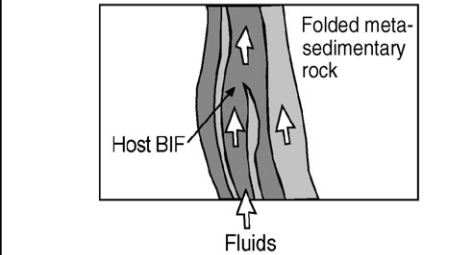

Fig. 1. Geographical location of The Granites and Dead Bullock Soak regions, Northern Territory (adapted from Adams, 1997).

Fig. 3. Summary of the styles of deposits observed in the Tanami Orogenic gold province (adapted from Wygralak et al., 2001), indicating different structural and lithological controls operating between The Granites and Dead Bullock Soak.

3. The Granites/Tanami aeromagnetic data

Because the Tanami Orogenic gold province is now largely covered by a veneer of regolith up to 100 m thick, mineral explorers have routinely acquired aeromagnetic data (e.g. Fig. 4) to better interpret the complex polydeformed geology.

An aeromagnetic survey encompassing the area from The Granites to the Dead Bullock Soak mines was flown during June/July 2001, using a fixed wing aircraft. The survey specifications were a sensor height of 20 m, a line spacing of 50 m, with 500 m tie lines. The instrument used was a Scintrex Cesium Vapour CS-2 magnetometer, with a sample rate of 0.1 s (10 Hz). The International Geomagnetic Reference Field (IGRF) has been removed from the observed Total Magnetic Intensity data to present residual anomalous values.

There are obvious highly magnetized groups of beds (Lower Blake Beds) at Dead Bullock Soak, showing a synform in the magnetic response (a: Fig. 4). In the eastern part of the magnetic image (636000E, 7727000N), contact aureoles surrounding granite intrusions have high amplitude (+1640 nT) residual magnetic signatures (d: Fig. 4). There are also linear magnetic highs at the Anomaly 2 (c: Fig. 4), Horden Hills (e: Fig. 4) and Magellan 2 (b: Fig. 4) prospects.

High amplitude (150–300 nT peak to peak) linear magnetic lows to the north of the magnetic highs are also of interest. Reduction-to-pole (RTP) of the residual magnetic field, failed to remove these low magnetic anomalies. After RTP, the induced magnetic anomalies should be symmetric; however, the magnetic lows do not conform to this pattern, instead being highly asymmetric, indicating probable remanent magnetizations within the magnetic source bodies.

The mineralogical sources of these negative anomalies have not previously been investigated, although these anomalies have been drilled during mineral exploration programs.

4. Magnetic mineralogy

The high amplitudes of the observed negative anomalies (hundreds of nT) in the aeromagnetic dataset demand that they are produced by ferrimagnetic minerals (part of the larger ferromagnetic group), rather than by paramagnetic mineral assemblages (Clark, 1997). Both pyrrhotite and magnetite are ferrimagnetic minerals that have been recorded previously in the Tanami region (Adams, 1997; Williams, 2002). Both can carry characteristic strong, spontaneous magnetizations and high susceptibilities (Clark, 1997).

Magnetite (Fe_3O_4) is the pure Fe-endmember of the titanomagnetite ($Fe_{3-x}Ti_xO_4$) group (Butler, 1992) and part of the larger group of Fe-rich ferromagnetic minerals with spinel structure (McIntyre, 1980). The distribution of the cations (Fe:Ti) in titanomagnetites gives distinctive magnetic properties. The Curie Temperature of pure magnetite (Fe_3O_4) is 578 °C; however this decreases to 200 °C or lower when significant Ti is present within the crystal (Clark, 1997).

Pyrrhotite includes different solid solutions of iron sulfides, and has the composition of $Fe_{(1-x)}S$, with $0 < x < 0.13$ (Dekkers, 1988; O'Reilly et al., 2000; Schwarz, 1975). There are three main crystallographic compositions of pyrrhotite: monoclinic, hexagonal and orthorhombic. Monoclinic pyrrhotite Fe_7S_8 (Zapletal, 1992) ($x = 1.25$) is ferrimagnetic, due to vacancy ordering (Rochette et al., 1990), whereas the hexagonal and orthorhombic compositions are antiferromagnetic, and compositionally close to Fe_9S_{10} ($x = 0.1$). These last two forms contribute little to the magnetic susceptibility of pyrrhotite-bearing rocks (Dekkers, 1988; O'Reilly et al., 2000), and cannot carry remanent magnetism (Zapletal, 1992). The Curie Temperature of monoclinic Fe_7S_8 is 325 °C (Dekkers, 1989), but can be as low as 310 °C due to slight variations in the Fe/S ratio (Dekkers, 1988; Schwarz, 1975).

5. Methods

In order to assess the possible contributors to regional-scale remanent magnetism in The Granites/Tanami Inlier, we employed alternating field (AF) demagnetization, Curie Temperature analyses, and hysteresis analysis. These results were combined with optical petrography and electron microscopy to determine the magnetic minerals present and their chemical compositions.

Thermal demagnetization and AF demagnetization can both be used to assess natural remanent magnetism (Clark, 1997). Curie
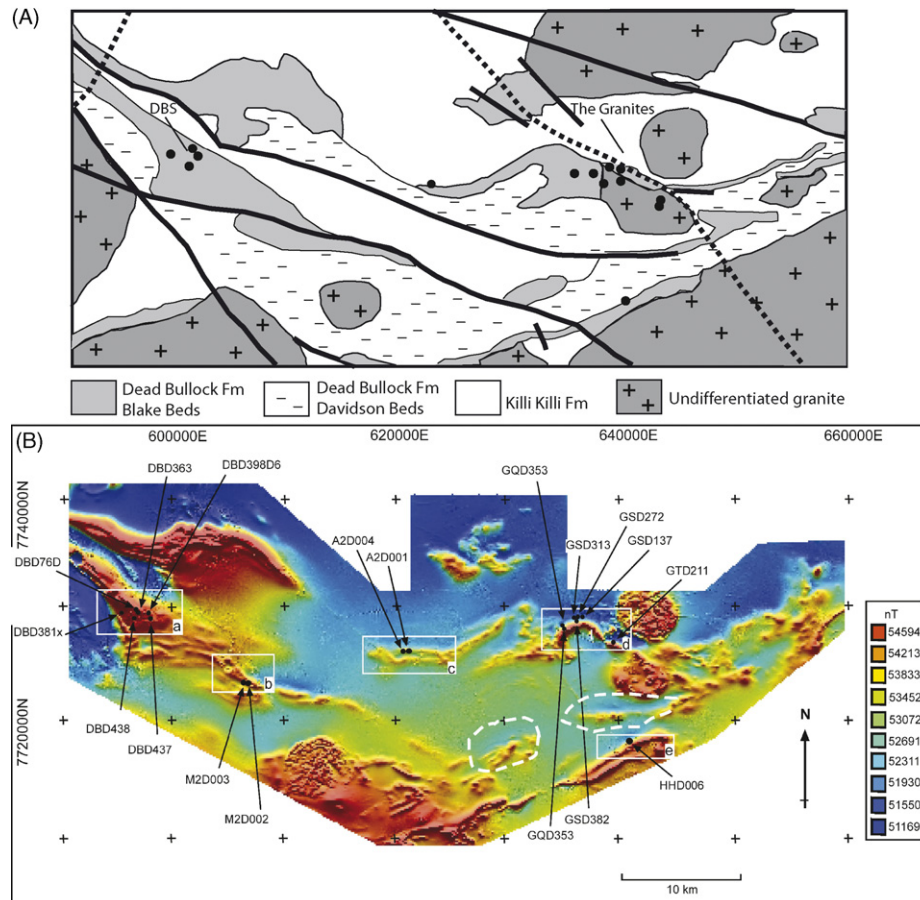
Fig. 4. (A) Interpreted regional geology (modified after Crispe et al., 2007); and (B) image of reduced to pole (RTP) total magnetic intensity (TMI) of The Granites/Tanami Inlier. Projection AGD84, Zone 52. Filled circles in A indicate sites of gold mineralization; Dead Bullock Soak (DBS) and The Granites goldfields are shown. Major regional faults are shown in bold; inferred faults are shown dashed.

In (B), the locations of the sampled drill holes are indicated at the different prospects throughout the Inlier (a, Dead Bullock Soak; b, Magellan 2; c, Anomaly 2; d, The Granites; e, Horden Hills). The region shows a mixture of magnetic highs and lows, with high amplitude negative magnetic anomalies circled in white.

Temperature analysis identifies minerals by the temperatures at which magnetic ordering disappears, and only paramagnetism remains. This property can be used to discriminate between possible sources of remanence, as each magnetized mineral has a distinctive Curie Temperature (Butler, 1992). Hysteresis analysis (e.g. Dunlop, 2002a,b) measures the ratios of the saturation remanent magnetization (Mrs) to the saturation magnetization (Ms), and coercivity of remanence (Hcr) to the coercive force (Hc). These properties are used to determine whether the remanent minerals are multidomain (typically > 10 μm), single domain ($\sim$1 μm), or pseudo-single domain (1–10 μm) grains in rocks where there are populations of mixed grain sizes (e.g. Dunlop, 2002a,b).

Optical petrography is used to determine the equilibrium mineral assemblages in the rocks, both to verify the presence of magnetic minerals, and to establish the parageneses in which they grew (e.g. primary, metamorphic, or alteration). Electron microprobing is used to observe chemical differences between minerals. If different generations of the same magnetized mineral are observed, microprobing of selected thin sections through a magnetic sample can distinguish whether there are chemical differences between remanent and non-remanent grains.

This suite of techniques has provided new insights into both the source of the unusual magnetic anomalies in the Tanami Orogenic gold province, as well as the timing of formation of these anomalies relative to metamorphic and hydrothermal events.

6. Results

6.1. Sampling

Extensive mineral exploration drilling programs throughout The Granites/Tanami Inlier intersected rocks spatially associated with the observed high amplitude negative magnetic anomalies (Fig. 4). Diamond drill holes sampled in our study were chosen for both high concentrations of magnetite and pyrrhotite, as recorded in drill logs based on visual inspection of cores, but also the spread of geographical locations of magnetic minerals recorded throughout the area (Table 1). Seven cores were examined from The Granites; one from Hordern Hills; two from Majellan 2; two from Anomaly 2; and six from Dead Bullock Soak (Fig. 4). Each drillcore was systematically measured for the downhole distribution of apparent magnetic susceptibility. Between three and eight samples were then taken from each core for petrographical, chemical and remanence analyses.

Two specific limitations of our sampling were associated with the legacy exploration core used. Firstly, the inclined cylindrical drillcores were not specifically oriented to denote up/down with respect to the surface when originally drilled. Secondly, for some drill holes, sufficient information was lacking to determine whether the drill holes were drilled vertically, or deviated. Because of these limitations, we were unable to determine the coherence and/or significance of remanent magnetization vectors measured in the

Table 1
Analyses of natural remanence, results show intense remanent magnetization, and differing inclinations and declinations

Drill holes	Easting, Northing AGD84, Zone 52	Strat Unit—observed minerals, (habit)	Depth (m)	Q	Intensity (A/m)	Susceptibility (10^{-5})	NRM declination (°)	NRM inclination (°)
GTD211	639035	SHIM—mt, po	157.5	0.61	23.86	76839	279	10.1
	7726732	SHIM—mt, po (s-c)	177.6	1.34	32.98	64314	104.2	−28.9
GQD353	634771	SHIM—mt, (po)	413.9	0.87	22.52	64547	222.1	−72.2
	7727966	SHIM—mt, po	418.3	0.66	3.52	12381	180.9	−74.2
		SHIM—mt, po	432.7	0.63	9.84	38896	231.3	−77.2
GSD313	635716	Orac—po (s-c)	298.8	9.25	33.97	10049	71.1	−37.6
	7728855	SHIM—mt, (po incl.)	311	4.04	13.65	11208	195.3	−70
		SHIM—mt, po	360.4	0.89	6.32	11276	353.6	68.5
GSD137	636342	Orac—mt, po	169.6	0.03	0.001	71.27	Weak/unstable	Weak/unstable
	7728894	SHIM—mt, (po incl.)	304.5	3.98	51.67	35053	128.9	−41.4
		SHIM—mt, po	307.5	4.68	33.83	22202	95.2	9.5
GSD272	635931	Orac—mt, po	241.4	0.23	1.98	22246	194.4	−57.1
	7728870	Orac—po, mt	291.45	3.85	1.76	1128	191.1	−45.7
		SHIM—po	314.9	1.08	1.75	4254	350.7	36.7
GSD382	635927	SHIM—mt, po	225.9	4.91	2.01	578	163.9	−70.3
	7728558	SHIM—mt, po	232.2	0.74	1.95	6295	242	−72
		SHIM—mt, (po incl.)	250.5	0.51	2.89	41942	258.6	−60.3
GQD296	634572	Orac—po (s-c)	275.4	18.35	25.68	2801	232	−49.4
	7728208	SHIM—po	301.3	7.58	79.56	1626	194.8	−56
		SHIM—mt, (?po)	321.15	0.78	5.15	38136	204.3	−76.9
M2D0002	606700	DB—po	160	7.87	2.14	835	167.1	−65.3
	7723400	DB—po (s-c)	198.2	10.73	28.29	5725	210.9	−55.9
		DB—mt, (po incl.)	208	3.99	4.6	3118	193.2	−56.3
M2D0003	606669	Orac—po (s-c)	121.2	28.43	35.1	6086	159.7	−63.9
	772337	Orac—po (s-c)	149.25	66.46	132.2	3659	36.9	28.5
		Orac—po	155.6	8.76	38.78	11850	212.5	−76.5
A2D0001	621160	MB—po (s-c)	226.4	50.86	40.94	2103	352.2	4.8
	7726062	SSS—po	249.35	6.54	2.19	855	145.1	−55.9
		MB—po	267.3	13.42	7.72	1460	178.2	−48.2
A2D0004	620761	?MB—po (s-c)	244.9	8.31	18.67	5649	250.8	−63
	7726111	?SSS—po, (mt)	258.3	5.62	0.38	154	158	−9.6
		?MB—po (s-c) (mt)	287.05	11.41	17.54	3897	192.3	−58.1
HHD0006	640540	DB (?SHIM)—mt	271.1	0.73	6.86	21461	177.6	−44.9
	7718156	BB—mt, (po incl.)	309	0.29	2.66	23825	224.2	−58
		BB—mt	344.7	0.36	4.16	28906	86.9	64.7
DBD363	596775	UBB—mt, (po incl.)	654.1	3.54	176.08	129525	175.9	−48
	7729288	UBB—po (?s-c)	685.05	16.6	238.82	29525	136.2	−13.8
		UBB—mt, (po incl.)	693.1	0.12	1.01	22142	274	−48.4
DBD381x	595203	LBB—mt	715.3	0.16	1.62	25304	65.4	−71.6
	7729440	LBB—mt	750.2	0.32	4.63	37728	269.2	−73.3
DBD76D	596455	LBB—mt, po	277.9	0.45	9.73	35930	99.1	−48.1
	7729657	LBB—mt, po	284.1	1.13	2.17	9531	241.1	−68.7
DBD437	597901	SHIM—mt	141.4	1.25	1.3	2581	179.1	−88
	7728930	SHIM—mt (po)	192	0.26	0.44	3534	43.1	75.6
DBD438	596338	SHIM—mt	160.8	5.6	180	80487	195.6	−84.9
	7728776	MB—po (s-c)	188.5	36.18	23.83	1784	73.9	−86
DBD398D6	597591	Orac—po (s-c)	558.3	22.2	16.86	6973	162.5	−79.8
	7729213	Orac—po (s-c)	573.4	51.75	91.11	4277	210.9	−78.1
		Orac—mt, (po incl.)	590	4.77	19.01	7244	173	−82.2

Each result is an average of three samples from the specified interval. Drill hole samples, indicating stratigraphic units shown in Fig. 9, and analyses of natural remanence, observed mineralogy, remanent magnetization, and NRM inclinations and declinations. Stratigraphic horizons (see also Fig. 2): BB, Blake Beds (includes Callie mine stratigraphy and Orac Fm: Smith et al., 1998); DB, Davidson Beds (includes The Granites mine stratigraphy: Adams, 1997); Orac, Orac Fm.; MB, Madigan Beds; SSS, Seldom Seen Schist Member; SHIM, Schist Hills Iron Member (part of DB); UBB, Upper Blake Beds; LBB, Lower Blake Beds; LBL, Lower Blake Lode. mt, magnetite; po, pyrrhotite. Habit of pyrrhotite: (s-c), mylonitic shear band; incl., inclusions in magnetite.

cores. Consequently, we present this orientation data without further analysis (Table 1).

6.2. Magnetic susceptibility

Reconnaissance magnetic susceptibility measurements of drill-cores were made using a Fugro GMS-2 hand-held magnetic susceptibility meter, in order to select magnetized material for further analysis. Readings were made over multiple 30 cm envelopes, in intervals where magnetite and pyrrhotite had been previously recorded in exploration company drill logs based on visual inspection. Drillcore was scanned using the hand-held meter to find the most magnetized intervals for sampling. Small (2 cm) cores were then cut from these intervals, and the magnetic susceptibilities

measured at the CSIRO laboratories, North Ryde. Observed susceptibilities in all cores ranged from 0.00007 to >1.2 (SI) (Table 1). Magnetic susceptibility measurements on core in the vicinity of regional high amplitude magnetic anomalies were strong, up to 1.53 (SI), and where remanent magnetization was suspected, magnetic susceptibility values ranged from 0.00057 to 1.4 (SI), averaging 0.167 (SI).

6.3. Optical petrography

Reflected and transmitted light optical petrography (Fig. 5) was undertaken on 38 samples from these magnetic intervals. All thin sections displayed metamorphic textures, either being porphyroblastic, or less commonly, poikiloblastic, i.e. with a matrix and large crystals, the latter occasionally with inclusions. This is consistent with the findings of Scrimgeour and Sandiford (1993), who evaluated metamorphic rock relationships in the study area.

In many thin sections, retrogressed and pseudomorphed garnets form porphyroblasts. Garnet is replaced by a chlorite–biotite–quartz ± ilmenite retrogressive mineral suite, with very little of the original mineral remaining. Pargasite, a blue-green sodic–calcic amphibole, is also found as porphyroblasts in several samples, and has the same crystal texture as muscovite growing alongside. The presence of pargasite has been previously interpreted as evidence of peak high temperature, low pressure metamorphic conditions (Scrimgeour and Sandiford, 1993).

The matrix in all samples is similar in modal composition (quartz–chlorite–muscovite–biotite–hornblende), with quartz the dominant mineral. There are abundant millimeter- to centimeter-scale quartz and quartz–calcite veins, varying in thickness and orientation (see also Adams, 1997). The transition of biotite to hornblende was also observed, confirming the observations of Scrimgeour and Sandiford (1993) that the rocks underwent greenschist to amphibolite facies peak metamorphism.

Under reflected light, magnetite and pyrrhotite dominate the opaque mineral assemblage, with trace amounts of pyrite, chalcopyrite and arsenopyrite. Magnetite shows different crystal forms in the study area (Fig. 5).

Type I magnetites are the most widespread. These are medium-fine (>10 μm) euhedral and subhedral porphyroblasts, and are typically inclusion-free (Fig. 5a). In contrast, Type II magnetites are retrogressed, relict poikiloblasts with pseudomorphed euhedral shapes, containing abundant inclusions of matrix quartz and micas (Fig. 5b). Type III magnetites, which are least common, are fine (ca. 10 μm) equant grains dispersed throughout the metasedimentary matrix.

The bulk of pyrrhotite observed in these samples forms subhedral grains in discrete millimeter-scale veins (Fig. 5c). These veins truncate the well-developed cleavage (s-planes), and have the form of shear bands (c-planes), an observation also confirmed by Adams (1997). The sulfide shear bands also cross-cut both garnets and amphiboles of the peak metamorphic assemblage. Fine and very fine-grained pyrrhotite is also present as diffuse selvages to these veins (Fig. 5c). Small amounts of pyrrhotite blebs can be found as rare inclusions in the Type I magnetite grains, indicating some minor pre-magnetite growth of pyrrhotite. Small magnetite inclusions can also be found within the main phase of pyrrhotite veins. This implies that there were at least two generations of pyrrhotite growth: one before, and one after the main stage of magnetite growth.

Ilmenite is present as very fine grains that overgrow retrogressed garnets (Fig. 5d) and within the principal tectonic foliation (see also Adams, 1997), indicating that they formed after peak metamorphism. Pyrrhotite and ilmenite are closely associated with

one another. Williams (2002) found that Ti was regionally liberated from titanomagnetites during the hydrothermal Au mineralising event, which may have led to ilmenite formation.

6.4. Electron microprobing

After optical analysis, 24 polished thin sections were selected for further investigation of their chemical compositions. This analysis was completed using the CAMECA SX51 Electron Microprobe at Adelaide University. An accelerating potential of 20 eV, beam current of 19.65 A and take off angle of 40 degrees was used for all analyses.

Results from these analyses are presented in Table 2. The main substituting cation in magnetite is typically Ti^{4+}, but Al^{3+}, Cr^{3+}, Mg^{2+}, Ca^{2+}, Mn^{2+} and Co^{2+} can also substitute (McIntyre, 1980); all of these elements were analysed with the microprobe. As pyrrhotite grains were also examined, S^{3-} was analysed along with Si^{4+}, Ni^{2+}, Zn^{2+} and As^{3+} (to detect traces of arsenopyrite in the samples). As these samples are near gold prospects, Au was also analysed; however the Au concentrations in the accessory magnetic phases were all below detection limit. Samples for which the addition of elements was more than 5% either side of 100 were discarded from subsequent stoichiometric calculations.

Type I and II magnetites are composed primarily of pure $Fe(ii)Fe_2(iii)O_4$, with negligible traces of Ca, Si, Al, Mg and Ti (Table 2). Williams (2002) also investigated this relatively pure magnetite, obtaining similar results. Ilmenite grains have Fe ≫ Mn, but there is little substitution of other elements (Table 2).

6.5. Remanent magnetism

What differentiates magnetic susceptibility and remanence is the time scale of the observation, and the presence or absence of an inducing field. In the laboratory, high frequency alternating magnetic fields can be applied to materials, and their effects gauged to determine magnetic susceptibilities (i.e. instantaneous magnetizations). Conversely, when determining magnetic remanence, no field is applied, and only longer term, permanent magnetization is detected. In between these states there are grains whose sizes allow thermal activation ("unblocking"), or for which very soft domain walls exist, and are free to move on an extended time scale of, say, days to years to millennia. Fortunately, the energy partitioning between these states is a sharp function of size and domain wall pinning, so the intermediate state (between laboratory and

Table 2
Stoichiometric analyses for distinguishing between the magnetite and ilmenite

Euhedral and subhedral magnetite	Ilmenite
Fe(ii)1.01Fe(iii)1.98Ti0.01Si0.01	(Fe2.19Mn0.09) Ti1.86
Fe(ii)1.12Fe(iii)1.76Si0.12	(Fe2.28Mn0.03) Ti1.85
Fe(ii)1.00Fe(iii)1.99Al0.01	(Fe2.08Mn0.12) Ti1.9
Fe(ii)1.02Fe(iii)1.94Ti0.02	(Fe1.34Mn0.79) Ti1.94
Fe(ii)1.01Fe(iii)1.98	(Fe2.20Mn0.027) Ti1.76
Fe(ii)1.00Fe(iii)1.99	(Fe1.56Mn0.73) Ti1.85
Fe(ii)1.00Fe(iii)1.99	(Fe1.36Mn0.81) Ti1.92
Fe(ii)1.01Fe(iii)1.98Si0.01	(Fe2.20Mn0.027) Ti1.76
Fe(ii)1.01Fe(iii)1.99	(Fe1.79Mn0.56) Ti1.83
Fe(ii)1.01Fe(iii)1.99	(Fe1.36Mn0.81) Ti1.92
Fe(ii)1.00Fe(iii)2.00	(Fe1.84Mn0.23) Ti1.96
Fe(ii)1.00Fe(iii)1.98	(Fe1.79Mn0.56) Ti1.83
Fe(ii)1.01Fe(iii)1.96	(Fe2.14Mn0.19) Ti1.83
Fe(ii)1.00Fe(iii)1.99	(Fe1.84Mn0.23) Ti1.96
Fe(ii)1.01Fe(iii)1.98	(Fe2.10Mn0.11) Ti1.9
Fe(ii)1.00Fe(iii)1.98Si0.01Ca0.01	(Fe2.14Mn0.19) Ti1.83
Fe(ii)1.00Fe(iii)1.99	(Fe2.13Mn0.06) Ti1.91
Fe(ii)1.01Fe(iii)1.92Si0.02Al0.02Mg0.01	(Fe2.10Mn0.11) Ti1.9

There is little substitution between elements, with the grains remaining pure.
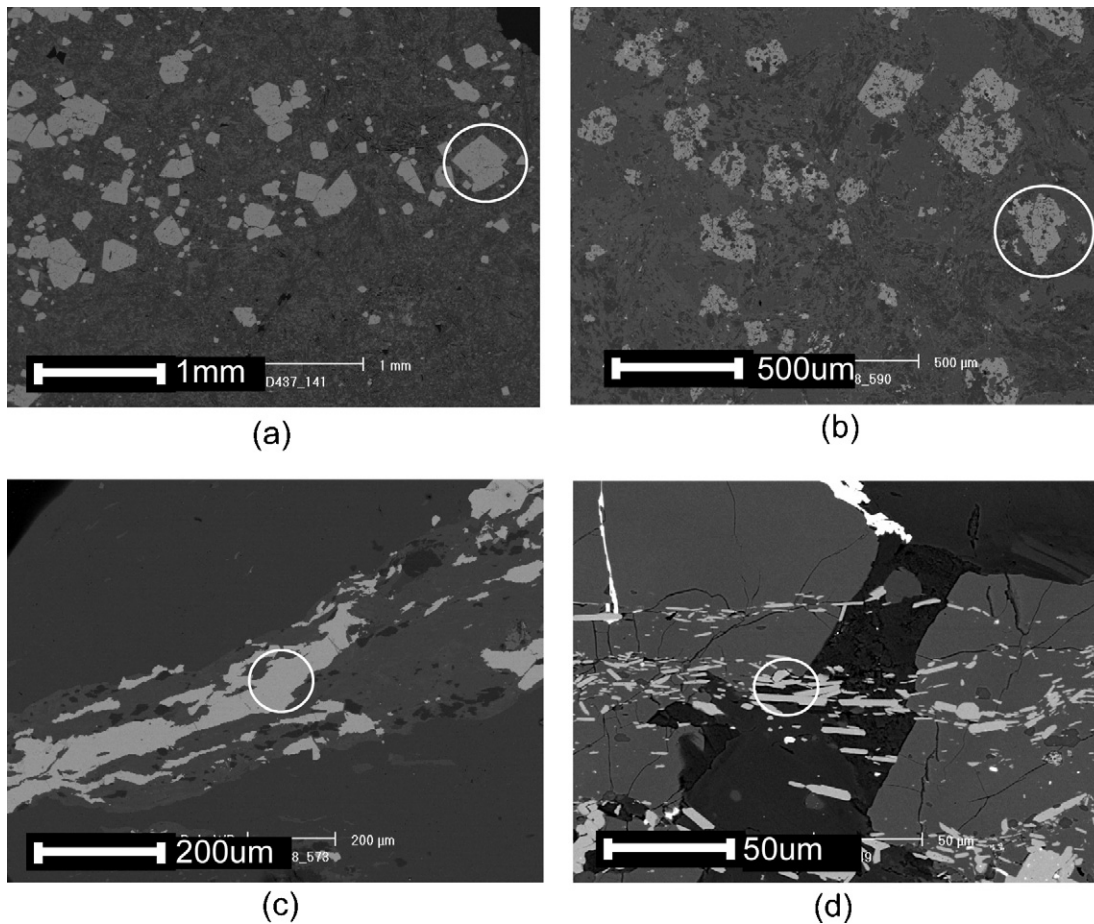
Fig. 5. SEM images of the main opaque minerals observed in the Tanami samples; (a) Type I magnetite, (b) Type II magnetite, (c) vein pyrrhotite and (d) very fine-grained ilmenite.

true geologic timescales) is ignored. This is why it is convenient to define magnetization as either induced or remanent, but it is worth remembering that, given enough time, all "permanent" remanence would "unblock" and thus, in principle, be indistinguishable from induced magnetization. It is also important to note that any remanent component parallel to the present day inducing magnetic field may also be indistinguishable from susceptibility in a conventional measurement, as the two components add vectorially to change only the amplitude of the measured response.

Natural remanent magnetizations (NRM) (Butler, 1992) can be divided into two subgroups, primary and secondary. Primary NRM is fixed during rock forming processes, but secondary NRM can occur anytime after primary NRM. It is sometimes the primary NRM that dominates the magnetic response; however, as primary and secondary NRMs add vectorially, secondary NRM can often obscure the primary NRM (Butler, 1992). In this study, the identification of primary (original) remanence is not as important as identifying the characteristic (most prevalent) component of remanence.

Forty-nine samples were cut into between three and seven cylindrical specimens 2.54 cm in diameter and 2.2 cm long. Measurement of NRM and AF demagnetization of NRM was carried out at CSIRO (North Ryde), using a 2G Enterprises model 2G600 with an in-line automatic AF system. For strong samples, remanent magnetizations were measured using a DIGICO fluxgate spinner with a sensitivity of about 10^{-4} A/m. The samples contained many sulfides, so thermal demagnetization was not carried out during AF demagnetization, as chemical changes occur within the sulfides during heating (e.g. Dekkers, 1989).

Data in Table 1 indicates that remanence contributes to the unusual negative anomalies in the Granites/Tanami Inlier (Fig. 4). Averaged intensities ranged from 0.001 A/m to 238.82 A/m (Table 1) with individual measurements (not shown) from the two end-member samples being as low as 0.0005 A/m and as high as 603.5 A/m.

The Koenigsberger Ratio (Q), defined as the ratio of remanent magnetization to induced magnetization, was also obtained for each sample. This ratio is a proxy for a rock's capability to retain a significant, stable remanent magnetization (Clark, 1997; McEnroe et al., 2001). The Q value of the samples in this study can be divided into three distinct classes: $Q < 1$, $1 \leq Q < 10$ and $Q \geq 10$. Samples with $Q < 1$ produce anomalies due to magnetic induction alone. For samples with $Q \geq 10$, remanent magnetism dominates the magnetic anomalies (Clark, 1997). For $1 \leq Q < 10$, both induced and remanent magnetizations influence the magnetic anomalies (Clark, 1997).

Fig. 6 shows that the Tanami sample suite would produce both induced anomalies and remanent anomalies. This figure also demonstrates regionally widespread remanent magnetizations, as high Q samples are found at each of the Dead Bullock Soak, The Granites, Magellan 2, Anomaly 2 and Horden Hills localities.

Zijderveld plots (Dunlop, 1979) showing representative AF demagnetization responses are shown in Fig. 7a and c, along with corresponding Curie Temperature plots (Fig. 7b and d). In the first sample type (Fig. 7a), there is a single, strong primary NRM component, defining a straight line, in this case from 10 mT to the origin. The independent heating curve for the sample indicates pyrrhotite is the remanence carrier. In the second example type (Fig. 7c), the
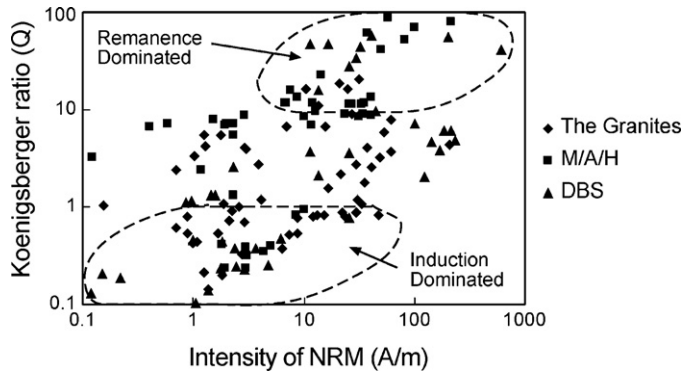
Fig. 6. NRM intensity plotted against the Koenigsberger Ratio (Q) for samples from Dead Bullock Soak, The Granites, and grouped samples from Magellan 2, Anomaly 2 and Horden Hills.

trajectory of the demagnetization trend does not decay towards the origin, indicating at least two components are present. The softer component, which may be viscous or other secondary remanent magnetizations, such as low temperature chemical remanent magnetization, could have formed during alteration or weathering. The harder component, while difficult to identify since it is harder than the highest AF demagnetization field available, appears to be

directed shallowly to the south. The reversible heating curve with a well-defined Curie point at 580 °C, indicates that magnetite is the magnetic carrier in this sample type.

6.6. Hysteresis analysis

Hysteresis analysis was conducted using data acquired on 3 critical samples (DBD438 160.8 m; DBD398D6 573.4 m; and DBD398D6 590.2 m). The procedure involves a small (maximum 200 mg) chip being ground to powder, and analysed at 25 °C with an alternating gradient force magnetometer at CSIRO (North Ryde). In our study, the three samples chosen for hysteresis analysis have mineralogical characteristics which allow the behavior of different compositions to be discretely evaluated.

Sample DBD438 160.8 m, had no pyrrhotite recorded during petrographic evaluation, and all opaque mineralogy is magnetite of various grain sizes, but includes very fine-grained Type III magnetite. This sample returned a Q value of 5.6, possibly indicating a contribution from remanence. On the Day Plot (not shown) this sample plots in the MD (Multi-Domain) magnetite field, with Mrs/Ms of 0.0934, and Hcr/Hc of 2.59295.

The other two samples analysed in this way were recognised petrographically as having mixtures of pyrrhotite and magnetite, presenting the possibility that remanent magnetizations in these
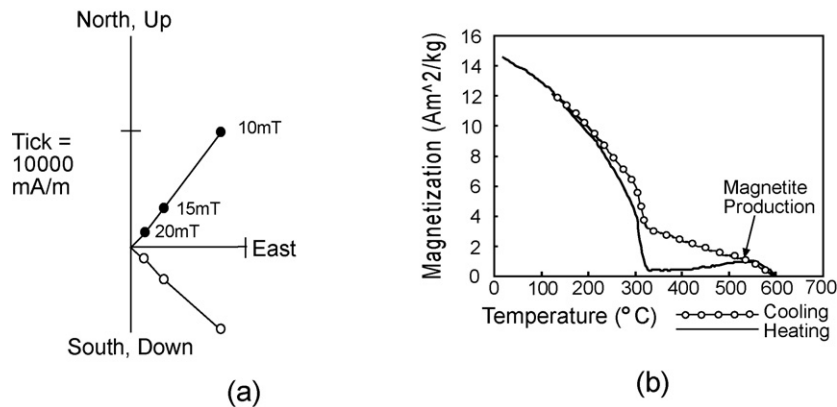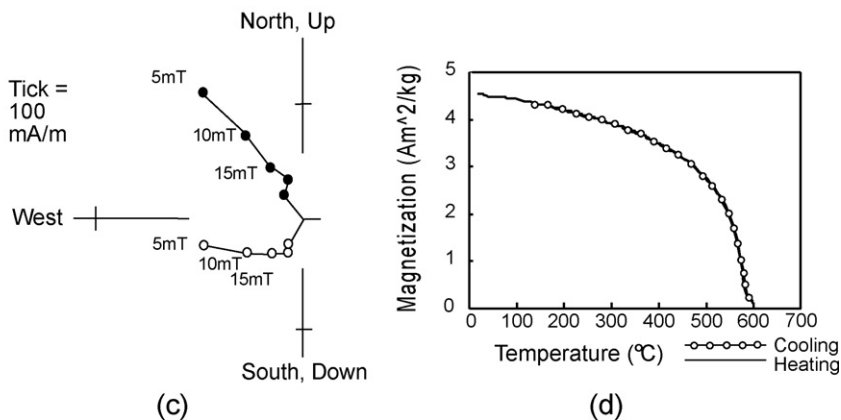

Fig. 7. Representative Zijderveld plots showing AF demagnetization trends (a and c) along with their corresponding Curie Temperature plots (b and d). Open circles represent projections onto the vertical plane, filled circles projections onto the horizontal plane. When magnetization is plotted against temperature, the main magnetic mineral is indicated. (b) Demonstrates the irreversible thermal demagnetizion of pyrrhotite whereas (d), with the reversible thermal demagnetization decreasing rapidly at 570 °C, indicates magnetite.

samples might be arising from PSD (Pseudo-Single Domain) behavior of Type III magnetites, rather than from pyrrhotite. Sample DBD398D6 573.4 m had an average Q value of 52, i.e. indicating strong remanence. Mineralogically, this sample is 95% pyrrhotite, with only minor ($\leq$5%) magnetite, and no Type III magnetites were found in this sample during petrographic analysis. On a Day plot, this sample would fall in the SD (Single Domain) field, with Mrs/Ms of 0.303218 and Hcr/Hc of 1.73571.

Sample DBD398D6 590.2 m has an average Q of 5, and is mineralogically 90% magnetite, probably including some Type III fine grains. On a Day plot, this sample would lie in the MD field, with Mrs/Ms of 0.100959 and Hcr/Hc of 3.84807.

These analyses invite the interpretation that it is the volume of pyrrhotite that is responsible for samples that have strong remanence. This is supported by the fact that for the sample with no pyrrhotite, the fine-grained Type III magnetites produced an MD response, rather than an SD response, as did a magnetite-dominated mixture. Both of these samples had Q values of around 5. Conversely, a pyrrhotite-dominated mixture with no Type III magnetites produced a SD response consistent with its very high Q value.

6.7. Curie Temperature

Six samples were analysed to determine their Curie Temperatures, using a Variable Field Translation Balance. Samples were heated stepwise in a field of 0.8 T and their magnetization monitored using a displacement transducer. The samples were chosen to evaluate the magnetic minerals contributing to the different populations of Koenigsberger Ratios within the sample set.

Samples with high Q ($Q \geq 10$) are dominated by remanently magnetized pyrrhotite (Fig. 7b), with the magnetization decreasing rapidly at 310–320 °C. This is accompanied by thermal alteration, resulting in the creation of minor magnetite at higher temperatures (*ca.* 570 °C). Upon cooling, the thermomagnetic curve is at a higher magnetization than that of its heating counterpart due to magnetite creation, a characteristic feature of pyrrhotite.

Samples with low Q ($Q < 1$) were dominated by magnetite (Fig. 7d), as the obvious slope down to zero magnetization at around 580 °C is indicative of the Curie Temperature of magnetite. The reversible thermomagnetic curve indicates the magnetite has not altered on heating, unlike the pyrrhotite-bearing samples. The low Q values are indicative of multidomain magnetite.

Two samples with intermediate ratios ($1 \leq Q < 10$) display mixed behaviors. A sample with Q of 1.6 has a curve indicative of multidomain magnetite (Fig. 7d). The other sample, with Q of 6.5, displays a large difference between the heating and cooling curves, i.e. an irreversible heating–cooling pattern. This result is similar to other samples with high Q values, where magnetite has been created by thermal breakdown of pyrrhotite (Fig. 7b). This indicates that samples with intermediate Q values contain both magnetite and pyrrhotite, which is consistent with the poikiloblastic textures observed in these samples.

7. Discussion

7.1. Magnetic mineralogy

Koenigsberger Ratios confirm that subhedral monoclinic pyrrhotite intersected in shear bands in widely spaced drill holes across The Granites/Tanami Inlier has a strong remanent magnetization. Fig. 8 demonstrates that every sample with Q greater than 10 has pyrrhotite as the dominant ferrimagnetic mineral. When magnetite dominates the magnetic mineral assemblage within a
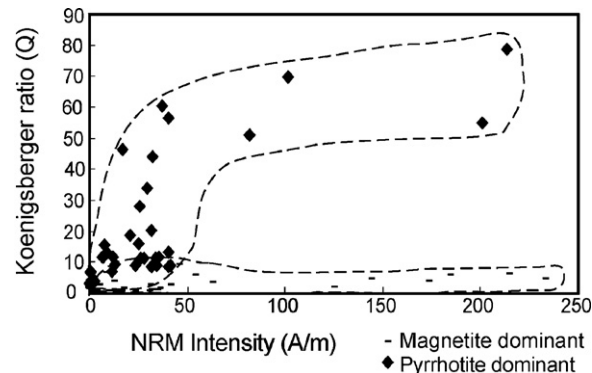

Fig. 8. Plotting the Koenigsberger (Q) Ratio against the natural remanent magnetism (NRM) intensity indicates there are discrete differences between the samples that have higher concentrations of pyrrhotite or magnetite.

given fabric (bedding or shear related), the Q values are all below 10, and mostly below 1; for the latter, induction responses dominate.

Type I magnetites, which are inclusion-free, euhedral and subhedral porphyroblasts are characteristic of recrystallised pelitic metasedimentary rocks (Rumble, 1976). These magnetites overgrow the distinct matrix foliation, but are also cross-cut by minerals related to the regional hydrothermal Au event (Williams, 2002). This suggests Type I magnetites formed at, or near, peak metamorphic conditions. In contrast, Type II magnetites, which show textural evidence of retrogression and reactions with the matrix, are most likely to be grains formed early in the prograde metamorphic path.

Analysing the Curie Temperature curves (Fig. 7b and d), and hysteresis data, neither Type I nor Type II magnetites contribute substantially to the observed high amplitude remanent magnetization. However, both magnetites have very high magnetic susceptibilities, and contribute to the high amplitude, induced regional magnetic anomalies observed in the aeromagnetic dataset.

7.2. Stratigraphic position of remanently magnetized minerals

The average Q values for the individual beds below the main Au-hosting Orac Formation (Fig. 9) are all less than 10. The main stratigraphic unit in the Tanami Orogenic Au province, the Blake Beds, therefore do not hold remanent magnetism. In contrast, strong remanence ($Q > 10$) is concentrated in the Davidson Beds and the Madigan Beds, in pyrrhotite-rich, magnetite-poor rocks. Correlation between stratigraphic units and pyrrhotite precipitation is likely to be due to fluid-wallrock buffering within discrete lithological units during the main sulfide forming phase of the hydrothermal Au event (e.g. Mikucki, 1998; Urbat et al., 2000). This explains the coincidence between magnetic remanence with certain favourable stratigraphic horizons, despite some later sulfide remobilization during regional shearing (Adams, 1997).

7.3. Magnetic mineral paragenesis

Magnetite in the study area grew either during diagenesis (Type III), prograde metamorphism (Type II), or at peak metamorphic conditions (Type I). In contrast, two discrete stages of pyrrhotite growth were observed. Early pyrrhotite blebs are included within (prograde) Type II magnetites, whereas pyrrhotite veinlets growing with ilmenite (Fig. 5d), demonstrably cross-cut syn-peak metamorphic garnet in the regional metamorphic foliation, consistent with post-peak metamorphic formation during greenschist facies retrogression.
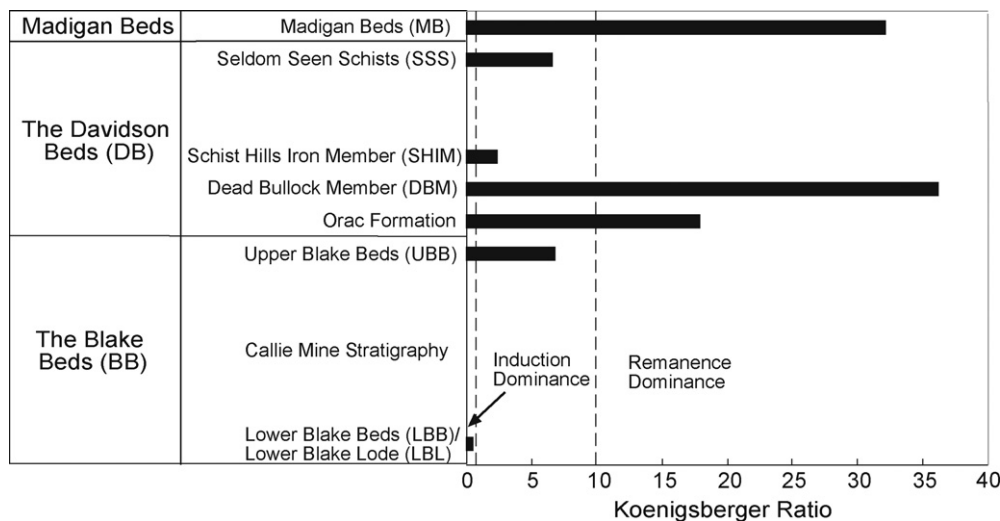
Fig. 9. The different lithological units with their corresponding Q values. Q > 10 is observed only in the Davidson Beds and Madigan Beds, suggesting a stratigraphic control on the distribution of pyrrhotite during the hydrothermal Au event.

At both The Granites, and Dead Bullock Soak, some early pyrrhotite and Type II prograde metamorphic magnetite formed in the rock mass, contemporaneous with multiple episodes of Au precipitation during the Tanami Orogeny and subsequent regional hydrothermal Au event (Adams, 1997). Adams (1997) observed that most pyrrhotite in the rock mass initially formed during a prograde metamorphic path, and was associated with arsenopyrite, loellingite, pyrite, chalcopyrite, marcasite, and a prograde metamorphic andalusite and garnet assemblage.

At, and slightly after, peak metamorphism (*ca.* 600 °C, 3.5 kbar: Scrimgeour and Sandiford, 1993), ductile pyrrhotite was subsequently remobilized along with pyrite, arsenopyrite, and Au. It forms the mylonitic sulfide shear bands that cross-cut peak metamorphic porphyroblasts (this study and Adams, 1997).

The equilibrium pyrrhotite–pyrite–arsenopyrite–chalcopyrite mineral assemblage (this study and Adams, 1997) has been shown elsewhere to form at temperatures of *ca.* 320–420 °C (Mikucki, 1998). Due to the low Curie Temperature of monoclinic pyrrhotite (325–310 °C: Dekkers, 1989), any strong TRM observed today must therefore relate to greenschist grade retrogression of the rock mass immediately following the hydrothermal Au event, which occurred over a long period after the thermal peak (>600 °C) of the Tanami Orogeny (Crispe et al., 2002).

Therefore, it can be concluded that remanence related magnetic lows observed in the aeromagnetic image (Fig. 4) is likely to map areas with higher proportions of structural layering (mylonitic shear bands) associated with the post-peak metamorphic sulfide and Au remobilization in the waning stages of the Tanami hydrothermal Au event. However, because of the distributed, ductile nature of the syn-to post-mineralization deformation which causes the structural interlayering of pyrrhotite and magnetite-bearing stratigraphy, it is not possible to uniquely associate the negative anomalies with zones of magnetite-free pyrrhotite mineralization. For this reason, we present no forward models of the architecture of the mineralization, as has been achieved by some authors working in upper crustal mineral systems (e.g. Alva-Valdivia et al., 2000, 2003c).

8. Conclusions

There is strong remanent magnetism in the vicinity of both The Granites and Dead Bullock Soak mines in the Tanami Oro-

genic Au province in northern Australia. Using a combination of petrographical, chemical, AF demagnetization, magnetic hysteresis and Curie Temperature analyses, we have determined that high remanence and low magnetic susceptibility is due to high concentrations of monoclinic pyrrhotite in certain stratigraphic horizons. This remanence likely formed during a regional-scale, post-peak metamorphic hydrothermal event, associated with Au and sulfide remobilization at temperatures of *ca.* 420–320 °C.

Euhedral and subhedral magnetites in the study area are typically prograde or peak metamorphic porphyroblasts, some with evidence of later retrogression. Both types are stoichiometrically pure magnetite, with negligible Ti in the magnetite structure. This is consistent with their formation prior to a regional Au mineralising event, which regionally stripped Ti from titanomagnetites (Williams, 2002). Rocks with high concentrations of magnetite display little or no remanent magnetism, but have high magnetic susceptibility, and produce induction-dominated magnetic anomalies.

Pyrrhotite is thus very important when interpreting magnetic signatures in regolith covered areas of the Tanami Au province. It may contribute to high positive amplitude magnetic signatures via moderate magnetic susceptibility, but is the main cause of high amplitude negative anomalies, due to its ability to hold strong, remanent magnetism. Because pyrrhotite occurs in a paragenesis with Au-bearing sulfides (pyrite, arsenopyrite and chalcopyrite), and has a Curie Temperature (*ca.* 325 °C) that only allowed remanent magnetization to survive following the cooler, waning stages of the regional hydrothermal Au event, remanent magnetic anomalies observed in aeromagnetic data must map structures associated with the post-peak metamorphic Au mineral system beneath the transported regolith cover.

References

Adams, G.A., 1997. Structural evolution and ore genesis of The Granites gold deposits, Northern Territory. Ph.D. Thesis, University of Adelaide, Adelaide.

Airo, M.-L., 2002. Aeromagnetic and aeroradiometric response to hydrothermal alteration. Surveys in Geophysics 23, 273–302.

Airo, M.-L., Loukola-Ruskeeniemi, K., 2004. Characterization of sulfide deposits by airborne magnetic and gamma-ray responses in eastern Finland. Ore Geology Reviews 24, 67–84.

Alva-Valdivia, L.M., Urrutia-Fucugauchi, J., Goguitchaichvili, A., Dunlop, D., 2000. Magnetic mineralogy and properties of the Peña Colorada iron ore deposit, Guerrero Terrane: implications for magnetometric modeling. Journal of South American Earth Sciences 13, 415–428.

Alva-Valdivia, L.M., Goguitchaichvili, A., Urrutia-Fucugauchi, J., 2003a. Petromagnetic properties in the Naica mining district, Chihuahua, Mexico: searching for source of mineralization. Earth, Planets, Space 55, 19–31.

Alva-Valdivia, L.M., Rivas, M.L., Goguitchaichvili, A., Urrutia-Fucugauchi, J., Gonzalez, J.A., Morales, J., Gomez, S., Henriquez, F., Nystrom, J.O., Naslund, R.H., 2003b. Rock-magnetic and oxide microscopic studies of the El Laco iron ore deposits, Chilean Andes, and implications for magnetic anomaly modeling. International Geology Reviews 45, 533–547.

Alva-Valdivia, L.M., Rivas-Sánchez, M.L., Gonzalez, A., Goguitchaichvili, A., Urrutia-Fucugauchi, J., Morales, J., Vivallo, W., 2003c. Integrated magnetic studies of the El Romeral iron-ore deposit, Chile: implications for the ore genesis and modeling magnetic anomalies. Journal of Applied Geophysics 53, 137–151.

Butler, R.F., 1992. Paleomagnetism: Magnetic Domains to Geologic Terranes. Blackwell Scientific Publications.

Clark, D.A., 1997. Magnetic petrophysics and magnetic petrography: aids to geological interpretation of magnetic surveys. AGSO Journal of Australian Geology and Geophysics 17, 83–103.

Clark, D.A., Tonkin, C., 1994. Magnetic anomalies due to pyrrhotite: examples from the Cobar area, NSW, Australia. Journal of Applied Geophysics 32, 11–32.

Crispe, A.J., Vandenberg, L.C., Cross, A., 2002. Geology of the Tanami region. Northern Territory Geological Survey Record 2002–0003.

Crispe, A.J., Vandenberg, L.C., Scrimgeour, I.R., 2007. Geological framework of the Archean and Paleoproterozoic Tanami Region, Northern Territory. Mineralium Deposita 42, 3–26.

Cross, A., Claoue-Long, J., Scrimgeour, I.R., Crispe, A.J., Donnellan, N.C., 2005. Summary of results. Joint NTGS-GA geochronology project : northern Arunta and Tanami regions 2000–2003 [electronic resource]. Northern Territory Geological Survey Record 2005-003. Northern Territory Department of Business, Industry and Resource Development, Darwin.

Dekkers, M.J., 1988. Magnetic properties of natural pyrrhotite. Part I: behaviour of initial susceptibility and saturation-magnetization-related rock-magnetic parameters in a grain-size dependent framework. Physics of the Earth and Planetary Interiors 52, 376–393.

Dekkers, M.J., 1989. Magnetic properties of natural pyrrhotite. Part II: high- and low-temperature behaviour of Jrs and TRM as function of grain-size. Physics of the Earth and Planetary Interiors 57, 266–283.

Dunlop, D.J., 1979. On the use of Zijderveld vector diagrams in multicomponent paleomagnetic studies. Physics of the Earth and Planetary Interiors 20, 12–24.

Dunlop, D.J., 2002a. Theory and application of the Day plot (Mrs/Ms versus Hcr/Hc) 1. Theoretical curves and tests using titanomagnetite data. Journal of Geophysical Research 107 (B3), 10.1029/2001JB000486.

Dunlop, D.J., 2002b. Theory and application of the Day plot (Mrs/Ms versus Hcr/Hc) 2. Application to data for rocks, sediments, and soils. Journal of Geophysical Research 107 (B3), 10.1029/2001JB000487.

Henkel, H., 1994. Standard diagrams of magnetic properties and density—a tool for understanding magnetic petrography. Journal of Applied Geophysics 32, 43–53.

Kelso, P.R., Banerjee, S.K., Teyssier, C., 1993. Rock magnetic properties of the Arunta Block, Central Australia, and their implication for the interpretation of long-wavelength magnetic anomalies. Journal of Geophysical Research 98, 15987–15999.

Kerim-Sener, A., Young, C., Groves, D.I., Krapez, B., Fletcher, I.R., 2005. Major orogenic gold episode associated with Cordilleran-style tectonics related to the assembly of Paleoproterozoic Australia? Geology 33, 225–228.

McEnroe, S.A., Brown, L.L., 2000. A closer look at remanence-dominated aeromagnetic anomalies: rock magnetic properties and magnetic mineralogy of the Russel Belt microcline-sillimanite gneiss, northwest Adirondack Mountains, New York. Journal of Geophysical Research 105, 16437–16456.

McEnroe, S.A., Robinson, P., Panish, P.T., 2001. Aeromagnetic anomalies, magnetic petrology, and rock magnetism of hemo-ilmenite- and magnetite-rich cumulate rocks from the Sokndal Region, South Rogaland, Norway. American Mineralogist 86, 1447–1468.

McIntyre, J.I., 1980. Geological significance of magnetic patterns related to magnetite in sediments and metasediments—a review. Bulletin of the Australian Society of Exploration Geophysicists 11, 19–32.

Mikucki, E.J., 1998. Hydrothermal transport and depositional processes in Archean lode -gold systems: a review. Ore Geology Reviews 13, 307–321.

Nicholson, P.M., 1990. Tanami gold deposit. In: Hughes, F.E. (Ed.), Geology of Australian and Papua New Guinean Mineral Deposits. The Australian Institute of Mining and Metallurgy, pp. 715–718.

O'Reilly, W., Hoffmann, V., Chouker, A.C., SoVel, H.C., Menyeh, A., 2000. Magnetic properties of synthetic analogues of pyrrhotite ore in the grain size range 1–24 μm. Geophysical Journal International 142, 669–683.

Pucher, R., 1994. Pyrrhotite-induced aeromagnetic anomalies in western Germany. Journal of Applied Geophysics 32, 33–42.

Rochette, P., Fillion, G., Mattei, J.-L., Dekkers, M.J., 1990. Magnetic transition at 30–34 K in pyrrhotite: insight into a widespread occurrence of this mineral in rocks. Earth and Planetary Science Letters 98, 319–328.

Rumble, D., 1976. Oxide minerals in metamorphic rocks. In: Rumble, D. (Ed.), Oxide Minerals: Reviews in Mineralogy, pp. R1–R24.

Schwarz, E.J., 1975. Magnetic properties of pyrrhotite and their use in applied geology and geophysics. Geological Survey of Canada Paper 74–59, 1–24.

Scrimgeour, I., Sandiford, M., 1993. Early Proterozoic metamorphism at The Granites gold mine, Northern Territory: implications for the timing of fluid production in high-temperature, low-pressure terranes. Economic Geology 88, 1099–1116.

Shive, P.N., Blakely, R.J., Frost, B.R., Fountain, D.M., 1992. Magnetic properties in the lower continental crust. In: Fountain, D.M., Arculus, R., Kay, R.W. (Eds.), Continental Lower Crust. Elsevier, pp. 145–170.

Smith, M.E.H., Lovett, D.R., Pring, P.I., Sando, B.G., 1998. Dead Bullock Soak gold deposits. In: Berkman, D.A., Mackenie, D.H. (Eds.), Geology of Australian and Papua New Guinean Mineral Deposits. The Australian Institute of Mining and Metallurgy, Melbourne, pp. 449–460.

Urbat, M., Dekkers, M.J., Krumsiek, K., 2000. Discharge of hydrothermal fluids through sediment at the Escanaba Trough, Gorda Ridge (ODP Leg 169): assessing the effects on the rock magnetic signal. Earth and Planetary Science Letters 176, 481–494.

Voulgaris, P., Emslie, J., 2004. Geology and ore estimation at the Callie underground gold mine, Tanami, NT. Australasian Institute of Mining and Metallurgy Bulletin 2, 71–78.

Whiting, T.H., 1986. Aeromagnetics as an aid to geological mapping—a case history from the Arunta Inlier, Northern Territory. Australian Journal of Earth Sciences 33, 271–286.

Williams, N.C., 2002. Controls on Mineralisation at the Callie Lode Gold Deposit, Tanami Desert, Northern Territory. Minerals and Geohazards Division, Geoscience Australia, Canberra, Professional Opinion (2002/09).

Wygralak, A.S., Mernagh, T.P., Fraser, G., Huston, D.L., Denton, G., McInnes, B., Crispe, A., Vandenberg, L., 2001. Gold mineral systems in the Tanami region. AGSO Research Newsletter 34, 2–9.

Zapletal, K., 1992. Self-reversal of isothermal remanent magnetization in a pyrrhotite (Fe_7S_8) crystal. Physics of the Earth and Planetary Interiors 70, 302–311.